Evaluation of ammonia-gasoline co-combustion in a modern spark ignition research engine

A Ambalakatte* 1, S Geng 1, A Cairns 1, A Harrington 2, J Hall 2, M Bassett 2

1Powertrain Research Centre, University of Nottingham, Nottingham, UK

2MAHLE Powertrain Ltd, Northampton, UK

*Corresponding Author name and email address

 Ajith Ambalakatte: ajith.ambalakatte@nottingham.ac.uk

 Jonathan Hall : jonathan.hall@mahle.com

ORCID ID

 A Ambalakatte : 0000-0002-1359-5440

 A Cairns : 0000-0001-6509-9986

ABSTRACT

Ammonia (NH_3) is emerging as a potential favoured fuel for longer range decarbonised heavy transport, particularly in the marine sector, predominantly due to highly favourable characteristics as an effective hydrogen carrier. This is despite generally unfavourable combustion and toxicity attributes, restricting end use to applications where robust health and safety protocols can always be upheld. In the currently reported work, a spark ignited thermodynamic single cylinder research engine equipped with gasoline direct injection was upgraded to include gaseous ammonia port injection fuelling, with the aim of understanding maximum viable ammonia substitution ratios across the speed-load operating map. The work was conducted at varied effective compression ratios under overall stoichiometric conditions, with the spark timing re-optimised for maximum brake torque at all stable logged sites. The experiments included industry standard measurements of combustion, performance, and engine-out emissions (including NH_3 "slip"). With a geometric compression ratio of 11.2:1, it was found possible to run the engine on pure ammonia at low engine speeds (1000-1800rpm) and loads of 12bar net IMEP. When progressively dropping down below this load limit an increasing amount of gasoline co-firing was required to avoid engine misfire. When operating at 1800rpm and 12bar net IMEP, all emissions of carbon (CO_2, CO, unburned hydrocarbons) and NOx decreased considerably when switching to higher NH_3 substitution ratios, with NOx reduced by ~45% at 1800rpm/12 bar when switching from pure gasoline to pure NH_3 (associated with longer and cooler combustion). By further increasing the geometric compression ratio to 12.4 and reducing the intake camshaft duration for maximum effective compression ratio, it was possible to operate the engine on pure ammonia at much lower loads in a fully warmed up state (e.g, linear low load limit line from 1000rpm/6bar net IMEP to 1800rpm/9bar net IMEP). Under all conditions, the indicated thermal efficiency of the engine was either equivalent to or slightly higher than that obtained using gasoline-only due to the favourable anti-knock rating of NH_3. Ongoing work is concerned with detailed breakdown of individual NOx species together with measuring the impact of hydrogen enrichment across the operating map.

KEYWORDS

Ammonia, IC engines, Combustion, Zero Carbon, E-fuels, Renewable Fuels, Maritime.

1   INTRODUCTION

The transportation sector is undergoing a renaissance in response to increasing pressures from global governments and society to reduce emissions of greenhouse gases and other pollutants resulting from the use of fossil fuels for power. While electrification is often the preferred solution to tackle this challenge, relative immaturity of battery technology, predominately associated lack of energy density, makes full electric propulsion unsuitable for heavy transport applications such as marine, off-road, rail and freight.

Ammonia (NH_3) has gained significant interest in recent years, both as a decarbonised energy vector and efficient hydrogen carrier. Volumetrically, liquid NH_3 can store ~45% more hydrogen than liquid hydrogen. Furthermore, NH_3 can be inexpensively stored as liquid (at -33°C at 0.1MPa or 0.86MPa at 15°C) and conveniently transported. Such promising characteristics have led many researchers to believe ammonia could become a key fuel for heavy transport provided key challenges around slow combustion and emissions control can be overcome [1, 2].

The concept of using NH_3 as a fuel in internal combustion engines can be traced back nearly a century, where it was used, for example, to run buses in Belgium during the 2nd World War [3]. This was followed by extensive research in the mid-1960s, where experiments were carried out in both Compression Ignition (CI) and Spark Ignition (SI) engines. Due to the high auto ignition temperature of NH_3, pure ammonia operation in CI engines is only possible with very high compression ratio (e.g. ~35:1) [4]. As a result, most studies in CI engines focus on "dual fuel" operation, where a pre-mixed ammonia-air mixture is ignited using a diesel-like pilot fuel of low auto ignition temperature and favourable cetane rating.

The dual fuel approach has been extensively researched with various fuels including diesel, dimethyl ether, kerosene and amyl-nitrate [5–12]. However, the added complexity of an additional fuel circuit, coupled with difficulties in operating the engines under throttled conditions and high carbon content of the pilot fuel, makes this solution less attractive for full replacement engines compared to SI engines. Compared to compression ignition, pure ammonia operation can be achieved in SI engines at considerably lower compression ratios as reported by Starkman et al. as early as the 1960s [13]. Pearsall et al. [10] investigated the operation with ammonia in both types of engines and recommended a high compression ratio (e.g. [12–16]) SI engine as an ideal solution.

While better than compression ignition, the relatively poor premixed combustion characteristics of NH_3 (see Table 1) makes it challenging to operate a SI engine with pure NH_3 at low loads. However, several strategies can be considered, such as increasing the effective compression ratio, supercharging (potentially without charge-air cooling), high ignition energy and co-fuelling with a faster burning sustainable fuel(s). Of these solutions, co-fuelling with hydrogen has been more extensively studied [14–19] due to excellent combustion characteristics combined with the ability to produce the hydrogen onboard via NH_3 "cracking" [20, 21].

Morch et al. [22] investigated the combustion of NH_3 at different hydrogen substitution levels and concluded that ~10% volume substitution yielded maximum thermal efficiency. Further to this, Firgo et al. [23] investigated ammonia-hydrogen co-fuelling at various speed/load conditions and concluded that combustion improvement from hydrogen enrichment had a reduced impact on engine speed extension compared to engine load. They further calculated the minimum amount of hydrogen energy required for stable combustion to be roughly ~7% for full load and ~11% for part load conditions. These researchers also investigated the feasibility of using exhaust gas heat to crack NH_3 on board and confirmed that hydrogen can be produced via the solution, however, the higher combustion temperatures required for the cracker resulted in significantly higher NOx emissions [24]. Recently, investigations conducted by Lhuillier et al. [25] and Mounaïm-Rousselle et al. [26] in modern SI engines also concluded that combustion of NH_3 can be greatly improved using small amounts of hydrogen (~10% vol) allowing the engine to operate at various loads and engine speeds ranging from 650rpm to 2000rpm.

Table 1 Combustion Characteristics of Ammonia and Hydrogen [27–31]

Species	Hydrogen	Ammonia	Gasoline
Chemical Formula	H_2	NH_3	$C_nH_{1.87n}$
LHV [MJ/kg]	120	18.8	44.5
Laminar Burning Velocity @ λ=1 [m/s]	3.51	0.07	0.58
Auto-ignition Temperature [K]	773-850	930	503
Research Octane Number	>100	130	90-98
Flammability Limit in Air [vol. %]	4.7-75	15-28	0.6-8
Quench Distance [mm]	0.9	22.07	1.98
Absolute Minimum Ignition Energy [mJ]	0.02	8	0.1
Latent Heat of Vaporisation [kJ/kg]	461	1369	350-400

Gasoline has also been studied extensively as a combustion promoter for NH_3 in SI engines, notably investigated by the CFR research group. Grannell et al. [32] investigated the fuel limits and efficiency of

ammonia-gasoline co-fuelling and concluded that ammonia can replace most of the gasoline energy above 4bar net Indicated Mean Effective Pressure (IMEPn), with the amount of gasoline needed reducing with increase in engine load and decrease in engine speed. Ryu et al. [33] investigated the direct injection of gaseous NH_3 into a Port Fuel Injected (PFI) gasoline engine and concluded that the long injection times needed for NH_3 negated any benefits of direct injection compared to PFI systems [34]. These researchers further conducted experiments with direct injection of cracked ammonia and found that the exhaust heat can be used to crack NH_3 on board without having significant impact on the performance and emissions of the engine. Haputhanthri et al. [35] studied the combustion of ammonia/gasoline emulsified mixtures and found that ammonia can be dissolved into gasoline using emulsifiers like ethanol and methanol and that the composite fuel could improve the performance of engine at high load conditions.

The goal of the current reported work was to undertake a baseline analysis of E10+NH_3 co-combustion in a modern high performance gasoline engine equipped with a modern combustion chamber layout and durable high energy ignition system designed for highly downsized SI engines (e.g. >30bar IMEP). It is drafted into 2 sections, the first section discuss the impact of effective compression ratio on co-combustion of E10-NH_3 mixtures, while the second section, discusses on the investigations conducted to identify the threshold loads where pure ammonia operation is possible at different engine speeds and delves further into the combustion, performance and emissions of pure ammonia operation over a range of speeds and loads.

2   EXPERIMENTAL SETUP

2.1   ENGINE HARDWARE

The experiments were undertaken in an externally boosted SI research engine which was a single cylinder derivative of the MAHLE Powertrain "DI3" demonstrator engine. The engine was equipped with a central spark plug and side mounted gasoline direct injector located under the intake valves for delivering standard UK pump grade gasoline (E10). Ammonia was delivered at the port via an upgraded manifold using a prototype Clean Air Power port fuel injector. The engine was also equipped with hydraulic fully independent variable valve timing to enable optimisation of valve timing and overlap. Set out in Table 2 are the key characteristics of the engine.

**Table 2 Engine hardware specifications**

Parameters	Value
Engine Type	Four Stroke Single Cylinder Spark Ignition
Displaced Volume [cc]	400
Stroke [mm]	73.9
Bore [mm]	83
Compression Ratio	• 11.33 • 12.39 (via Piston Swap)
Number of Valves	4
Valvetrain	Dual Independent Variable Valve Timing (40°CA Cam Phasing)
Fuel Injection Configuration	• Side DI Gasoline (E10) • PFI Ammonia
Max Fuel Injection Pressure [bar]	175 (gasoline)
Cylinder Head Geometry	Pent-Roof (high tumble port)
Piston Geometry	Pent-Roof with Cut-outs for Valves
Ignition Coil	Single Fire Coil, 100mJ, 30kV
Max Power [kW]	40 (gasoline)
Max IMEPn [bar]	30 (gasoline)
Max In-cylinder Pressure [bar]	120
Max Speed [rpm]	6800 (limited by valve train) 0
Boost System	External Compressor (Max 3bar gauge)
Control System	MAHLE Flexible ECU
Interface Software	ETAS INCA

The initial tests were conducted using a geometric compression ratio of 11.33 with longer opening cams typical of GDI multi-cylinder engines with high valve overlap potential for low-speed performance, with the engine capable of operating using 100% ammonia in this configuration at limited sites. In later work the piston was replaced to elevate the geometric compression ratio to 12.39, while also adopting shorter duration cams to maintain a high effective compression ratio (volume of cylinder at intake valve closing/ clearance volume). The details of the engine upgrade and resulting improvements in effective Compression Ratio (CR) and effective Expansion Ratio (ER) for the same valve overlap is given in Table 3.

**Table 3 Improvements to Effective CR and Effective ER with engine upgrades**

Parameters	Value	
Overlap [CAD]	37	
Geometric Compression Ratio	11.33	12.39
Cam Reference	"Old"	"New"
IVC [a] [CAD]	580	564
IVO [a] [CAD]	340	344
EVC [a] [CAD]	378	388
EVO [a] [CAD]	113	154
Effective CR	10.3	12.02
Effective ER	8.60	11.94
[a] Crank angle where valve lift is 0.1mm		
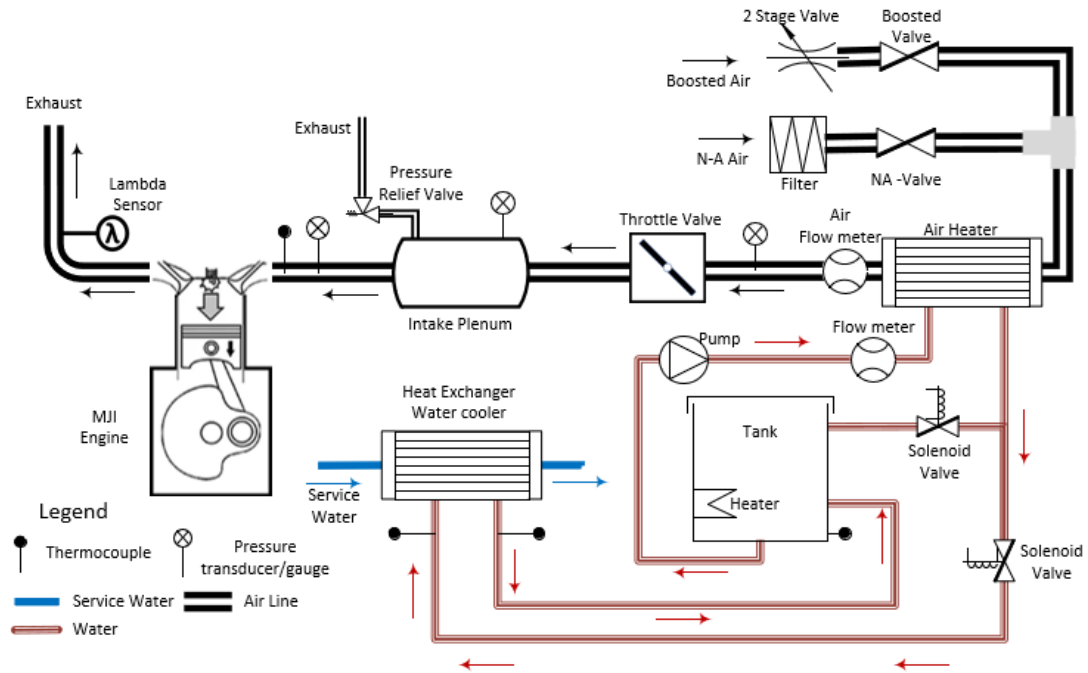
Figure 1 Schematic of the test rig gas path and coolant control

Schematics of the intake air system and the ammonia supply system are shown in Figures 1 and 2 respectively. The engine could be operated as either naturally aspirated or boosted using an external compressor rig providing up to 3bar gauge boost pressure. The temperatures of the intake air (45^{0}C), engine coolant (95^{0}C) and oil (95^{0}C) were maintained at a constant value (±1°C) using dedicated conditioning circuits. Furthermore, surge tanks were added to both the intake and exhaust to minimise the effects of unwanted gas pressure fluctuations.
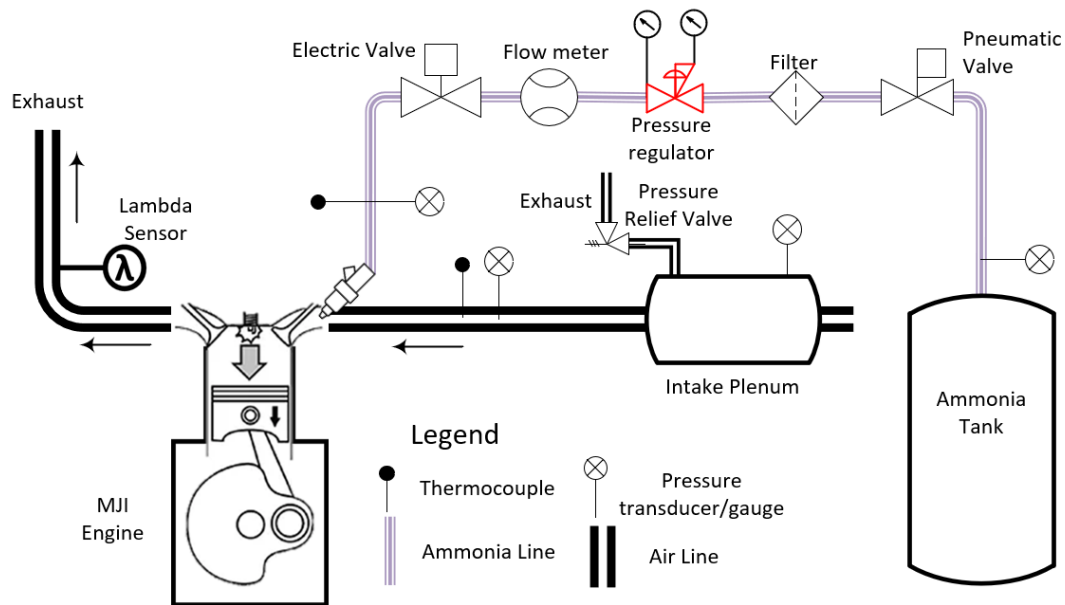
Figure 2 Schematic of the engine fuel supply line

The ammonia was supplied to the engine in gaseous phase using a dedicated port injector supplied by Clean Air Power. The NH_3 was stored in liquid vapour equilibrium via a drum, with the pressure differential between the intake manifold and vapour pressure inside the drum used to drive the supply of ammonia to the engine. The flowrate of NH_3 was measured using a Coriolis flowmeter procured from Micro-motion (maximum flow rate error of 1% at the minimum flow rates reported). Electrically controlled safety valves and nitrogen-based purging were added to the supply line to isolate the ammonia supply in the case of an emergency. For the gasoline supply, an AVL 735 fuel balance unit was used to measure the gasoline (E10) flowrate and condition the gasoline temperature (20°C set point) before being fed to a high-pressure fuel pump at constant supply pressure via a fuel regulator.

In-cylinder pressure was measured using a Kistler 6045-B piezo electric pressure transducer working through a AVL Micro-FEM amplifier, which was fully calibrated in-situ to industry standards via a dead weight tester. The intake and exhaust pressures were also measured using Kistler's 4045A and 4011 piezo resistive transducers. The engine-out emissions were measured using a series of dedicated analysers from the Signal group, in addition to industry standard emissions (NOx, CO_2, CO, THC and O_2) ammonia "slip" emissions (unburned NH_3 in the exhaust) were also measured based on a new Signal unit. The details of the emission analysers are summarised in Table 4. All measurements were recorded and processed using a bespoke National Instruments Data Acquisition system. The data from the pressure transducers was recorded at a resolution of 0.2 Crank Angle degrees (CAD) using a Hohner 3232 optical encoder, which was synchronised using an AVL capacitive probe. During testing 300 cycles of pressure data were recorded at every site. Mass fractions burned were evaluated on a qualitative basis using one dimensional heat release analysis. Other "steady state" temperature, pressure and flow measurements were recorded at a frequency of 10Hz.

Table 4 Details of the emission analysers

Equipment	Gas	Operating Principle	Dynamic Range	Accuracy / Error(%)
4000 VM	NOx	Chemiluminescence	0-10000 ppm	Better than +1% range or ±0.2 ppm whichever is greater.
8000 M	O_2	Dumbbell paramagnetic sensing	0 -5 %, 0 -10 %, 0 -25 %	±0.01 %O2.
S4 Nebula	NH_3	Tuneable Diode laser Spectrometry	1ppm -10,000 ppm	±2% of FDS
3000 HM	THC	Flame ionisation detector	0-10000 ppm	Better than ±1 % range or ±0.2 ppm whichever is greater.
7000 FM	CO, CO_2	Infra-red gas filter correlation technique	100-10000 ppm Or 1-100 %	Better than ±1 % of range or ±0.5 ppm whichever is greater.

2.2 TEST PLAN

Since practical applications of ammonia are expected to be in low-to-medium speed heavy duty engines, the test points were selected to cover typical peak power speed ratings for such engines. Initial tests were

conducted at 12bar IMEPn and 1800rpm with the aim of determining the minimum co-fuelling required to stably operate the engine on ammonia. The co-fuelling required was evaluated by undertaking ammonia "displacement sweeps"; with the engine first fired using pure E10 and NH_3 progressively added until an upturn in combustion stability occurred (with repeat logs around this upturn to establish the maximum possible NH_3 substitution and the upper limit set to a coefficient of variation in IMEP of >3%). All logs were obtained under stoichiometric conditions with the spark timing set to Maximum Brake Torque (MBT). In early work it was proposed that slightly rich running might aid NH_3 displacement (due to slightly higher laminar burning velocity), but this was not found to be the case; with the engine misfiring more easily when attempting to operate slightly richer when at the substitution ratio limit due to the relatively low relative air-to-fuel ratio of NH_3 and significant reduction in the ratio of specific heats (and hence gas temperature) "over-ruling" relatively small increases in laminar burning velocity when slightly rich. Such effects were previously insinuated by the chemical modelling work of Kobayashi et al.[36]. Further to displacement sweeps at 1800rpm and 12bar IMEPn, load sweeps at constant speed and speed sweeps at constant load were completed to crudely understand how co-fuelling influenced the engine operation.

The engine settings used for the tests are set out in Table 5. In addition to these settings, the valve timing was fixed for the tests, however, the overlap was adjusted from 37 Crank Angle Degrees (CAD) to 24 CAD for the 1000rpm tests as the slow speed combined with high boost pressure otherwise resulted in significant ammonia slip, due to high apparent cylinder scavenging at this speed.

Table 5 Engine settings for substitution tests

Settings	Values
Operating Temperature (Coolant & Oil) [^{0}C]	95
Spark Timing	Maximum Brake Torque (MBT)
Air-fuel Equivalence ratio	1
E10 Injection Start angle [CAD BTDCf]	310
Ammonia Injection End angle [CAD BTDCf]	400
Inlet air temperature [^{0}C]	45
Ammonia rail pressure [barG]	3-5
Ammonia Feed Temperature [^{0}C]	27 - 30
E10 Temperature [^{0}C]	20
Stability limit	Coefficient of variation (CoV) of IMEPn >3%

3 RESULTS

3.1 EFFECT OF COMPRESSION RATIO AND SHORTER CAMS ON AMMONIA OPERATION.

3.1.1 MAXIMUM AMMONIA DISPLACEMENT

The maximum displacement of ammonia achieved via a speed and load sweep is shown in Figure 3, where the number in the "bubbles" denotes the maximum percentage of ammonia substitution where stable combustion could be maintained. The improvements in compression ratio reduced the threshold engine load needed to achieve 100% substitution from 12bar IMEPn to 10bar IMEPn at 1800rpm. Furthermore, the higher compression ratio also improved the substitution by ~10% at the lower load points, except at 1800rpm/8bar IMEPn where the recorded improvement was only 2%. The increase in load beyond 12 bar IMEPn was restricted by the fuel supply line, which is the cause for the 90% substitution at 14 bar IMEPn in the low CR configuration. These challenges were rectified with higher CR upgrade and further tests were conducted with the higher CR hardware at 1000 and 1400 rpm, where 100% operation were achieved at lower IMEPn, these results are discussed in the following section 3.2 and 3.3 respectively.
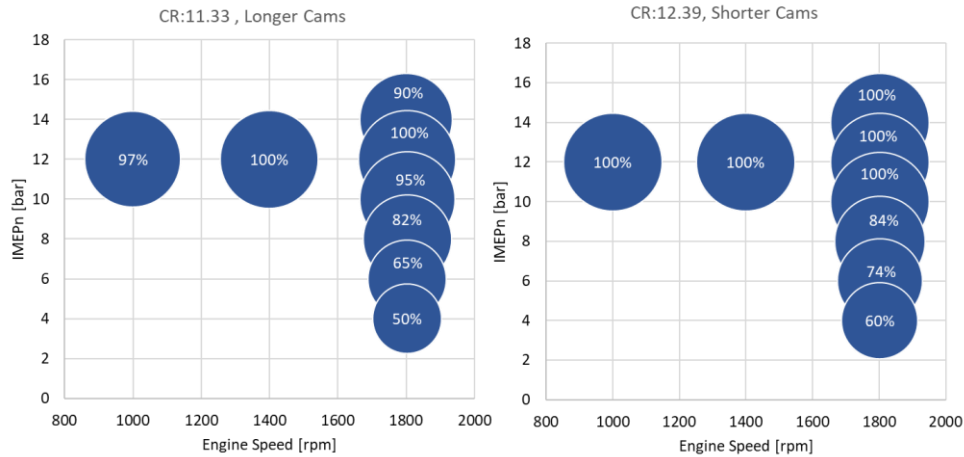
Figure 3 Comparison of maximum ammonia substitution achieved at varied compression ratio during speed and load sweeps (λ=1, optimised spark timing)

To understand the improvements brought about by the higher CR, further ammonia substitution sweeps were conducted at 1800rpm/12bar IMEPn with the new hardware with the aim of understanding how CR affects the combustion, performance, fuel economy and emissions of the engine.

3.1.2   COMBUSTION

The spark timing required to achieve MBT operation and associated combustion stability is set out in Figure 4. As seen in the figure, the spark timing is identical for all test points above 50% ammonia energy fraction, while it deviates at lower energy fractions, it is only significant with pure E10 operation (0% ammonia energy fraction in diagram). Due to knocking with pure E10 operation, the spark timing was retarded from MBT to one crank angle degree before persistent detonation, termed as "Borderline Detonation-1 (BLD-1)". For the higher CR hardware, BLD-1 spark timing was considerably more retarded than the lower CR hardware due to the higher in-cylinder gas temperatures.

Examining the values of coefficient of variation (CoV) of IMEPn, the engine operation was relatively stable for the higher CR configuration, with the threshold load for pure ammonia operation reduced to 10bar IMEPn as opposed to 12bar IMEPn with the lower CR configuration.
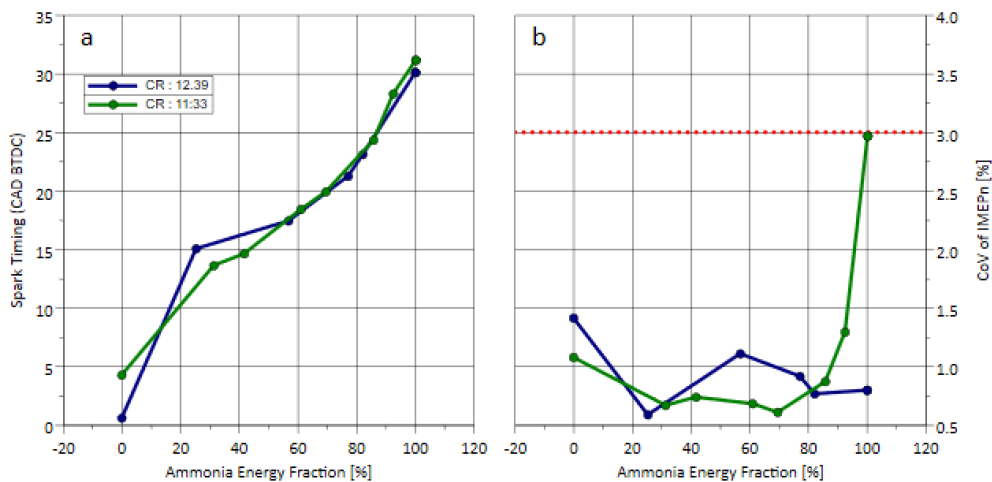
Figure 4 Variation (a) Spark timing (b) CoV of IMEPn for various ammonia substitution for both hardware

The impact of ammonia addition on combustion can be analysed using the traces of in-cylinder pressure and rate of heat release (RoHR) given in figure 5 and 6 respectively. Only 3 displacement points namely pure E10 (0% NH_3), co-fuelling (60% NH_3) and pure NH_3 (100% NH_3) were plotted as the variation of data in the co-fuelling region seems identical for both CR configuration. The favourable anti-knock characteristics of NH_3 coupled with the high E10 content enables the co-fuelling case (red) to achieve the highest in-cylinder pressure in both configurations. BLD-1 spark timing in case of pure E10 (blue) operation results in gradual pressure rise and lower peak pressures due to the combustion mostly occurring in the power stroke. While the pure NH_3 (green) operation achieves higher peak pressures than pure E10 operation, the slow combustion of ammonia results in a gradual pressure rise than the co-fuelling case even with 10CAD advance in spark timing. Between the 2 CR configurations, the higher CR configuration achieves higher peak pressures and pressure rise rates

than the Lower CR when ammonia is present in the fuel mix. Furthermore, the benefit of higher CR is only evident in pure NH$_3$ operation, where pressure rise rate is significantly better than lower CR configuration compared to both co-fuelling and pure E10 operation. The improvements in the effective expansion ratio, brought about by the change in cams can also be seen in the pressure traces with the higher CR tests retaining more pressure after 480 CAD than the lower CR configuration.
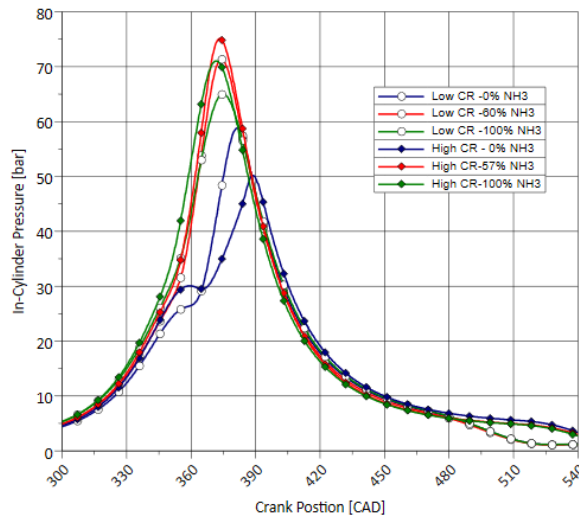
Figure 5 In-Cylinder pressure traces for both configuration with 0%, 60% and 100% ammonia displacement

Analysing the RoHR traces in figure 6 gives a better insight into the better pressure rise rate of the higher CR configuration for pure NH$_3$ operation. Even with slightly advanced spark timing, there is considerable delay (~20 CAD) to start of heat release in the lower CR configuration owing to the lower pressure and temperature inside the cylinder at the ignition moment. This improved initial phase of combustion results earlier and higher peak heat release rate for the higher CR configuration. However, pure NH$_3$ operation have notably lower peak heat release rate compared to pure E10 and co-fuelling case. Furthermore, the improvements in initial phase of combustion are also absent for the higher CR configuration for the co-fuelling case with both heat release traces being nearly identical. Compared to pure NH$_3$ tests, the heat release curves for pure E10 tests are reversed with the lower CR configuration having better heat release by virtue of advanced BLD-1 spark timing compared to the higher CR configuration. While the higher CR achieves a peak heat release rate, the drop-in heat release rate in far more rapid compared to both co-fuelling and pure NH$_3$ operation with the latter having a gentler drop in the heat release rate.
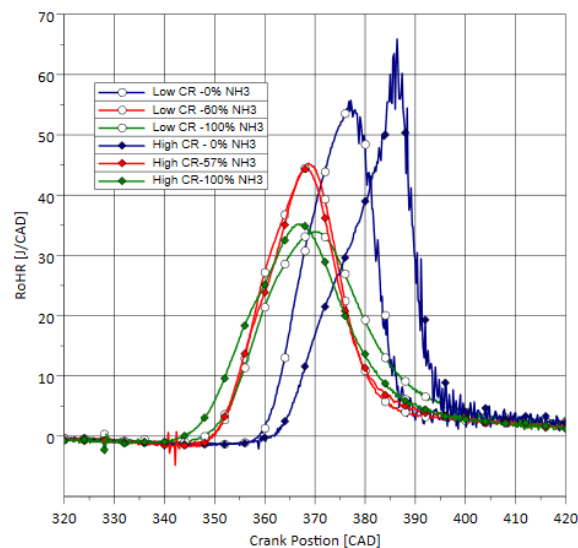

Figure 6 RoHR traces for both configuration with 0%, 60% and 100% ammonia displacement

While there is an improvement in the combustion for the Higher CR configuration, it doesn't translate into an improved spark timing which can examined by analysing the Mass Fraction Burned (MFB) data shown in Figure

7. As seen in the figure, the "flame development phase" (0-10% MFB) given in Figure 7(a), shows an improvement of ~4 CAD for the higher CR configuration compared to the lower CR configuration. This suggests that the higher CR configuration aids in the initiation of combustion for pure ammonia operation. However, this improvement is negated by the addition of auxiliary fuels (E10 in this case), as the values of 0-10% MFB are identical for both configurations when the engine is operated with a combination of both fuels. Furthermore, the "combustion phase" (10-90% MFB) duration set out in Figure 7(b) is longer for the higher CR configuration under all substitution points, potentially implying a faster combustion can be achieved via a lower CR configuration with fuel enhancement.
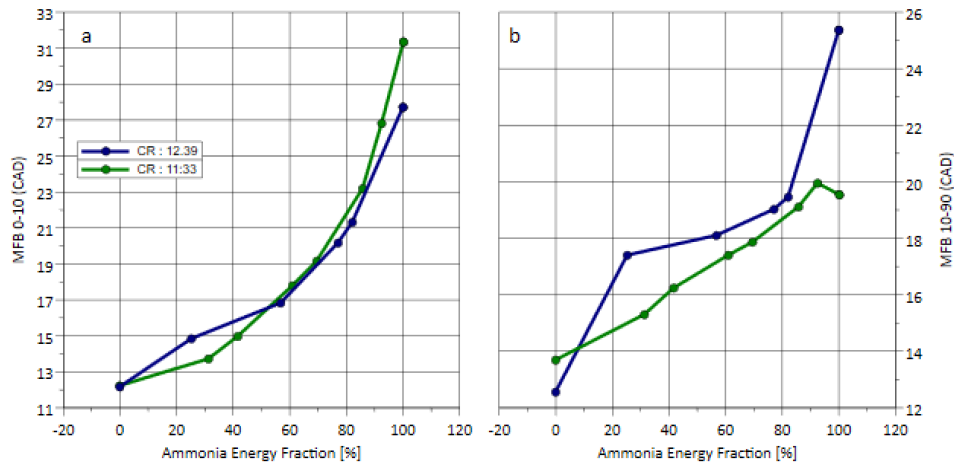
Figure 7 Variation of (a) 0%-10% MFB (b) 10%-90% MFB for various substitution rations in both configurations

One potential explanation for the longer MFB 10-90% higher CR configuration is the delayed combustion of ammonia trapped in the crevice volumes of the piston. This hypothesis can be evaluated using the data of angle of maximum cylinder pressure (Pmax) and 90% MFB timing (CA90) shown in Figure 8.
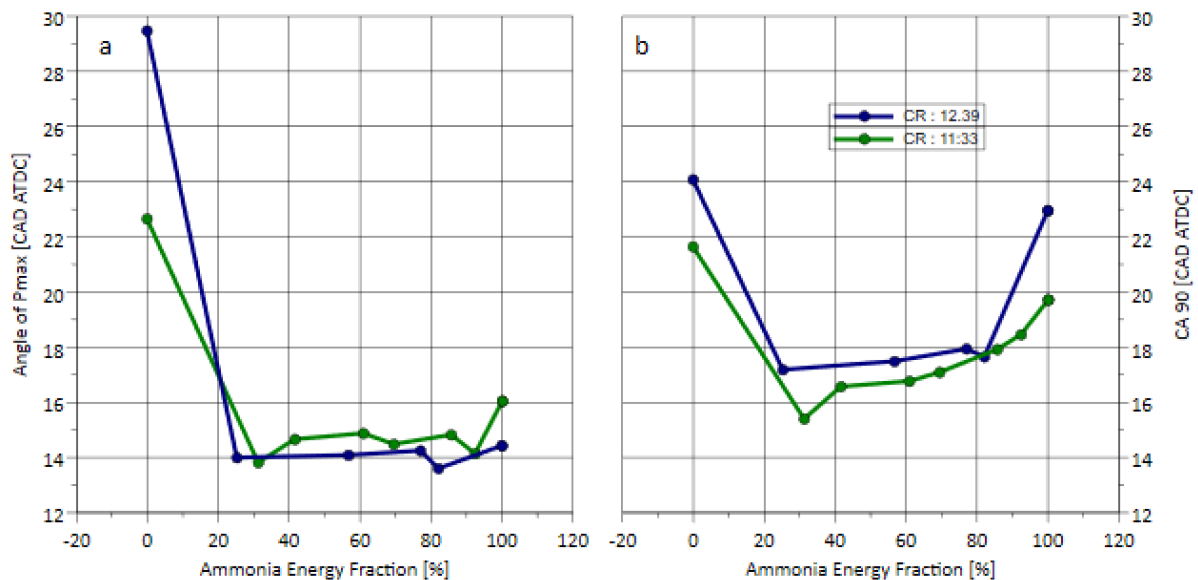

Figure 8 Variation of (a) Angle of Pmax (b) CA90 for various substitution ratios in both configurations

As depicted in the diagram, the pressure within the cylinder reaches its peak well before the 90% MFB is reached indicating some of the unburned mixture trapped in the crevice volume escapes the main combustion event but is burned as the piston moves down during the early power stroke. For the higher CR configuration, the amount of unburned mixture trapped in the crevice volume could be higher owing to higher in-cylinder pressure, as indicated by the data in Figure 10(b) below. This in-turn would lead to more ammonia being burned after the peak of in-cylinder pressure resulting in the longer MFB 10-90% duration.

3.1.3 EFFICIENCY

The indicated thermal efficiency achieved via both configurations is shown in Figure 9(a), where the efficiency can be seen to be considerably higher for the high CR configuration, achieving nearly 40% compared to ~36% for the low CR setup. However, this improvement in efficiency should be attributed to the shorter exhaust cams that open later in the power stroke thereby increasing the effective ER from 8.6 to 11.94 and extracting more work from the combusted gas as seen from the pressure-volume (p-V) diagram shown in Figure 9(b) (depicting the average cycle over 300 firing cycles for each case).
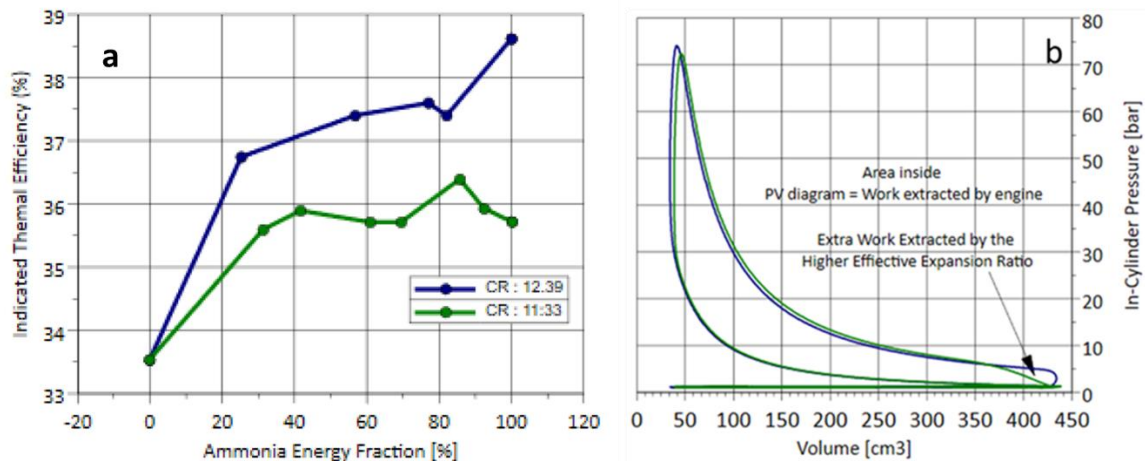
Figure 9 (a) Indicated thermal efficiency variation and (b) PV diagram of a cycle in both configurations

3.1.4 EMISSIONS

One of the negative impacts of the higher compression ratio is increased NOx emissions, as shown in Figure 10(a). The tests conducted with the higher compression ratio hardware exhibited ~1000ppm higher NOx than the low compression ratio hardware. Since the spark timing is identical for both hardware setups, the peak cylinder pressures (and hence peak temperatures) tend to be higher for the higher compression ratio engine, as shown in Figure 10(b). As a result, the higher compression ratio hardware develops a more suitable environment for thermal NOx formation Furthermore, the NOx emissions reduce with increased ammonia displacement, reducing by 57% from pure E10 to pure ammonia operation even when pure E10 operation is has lower maximum cylinder pressure from the retarded spark timing
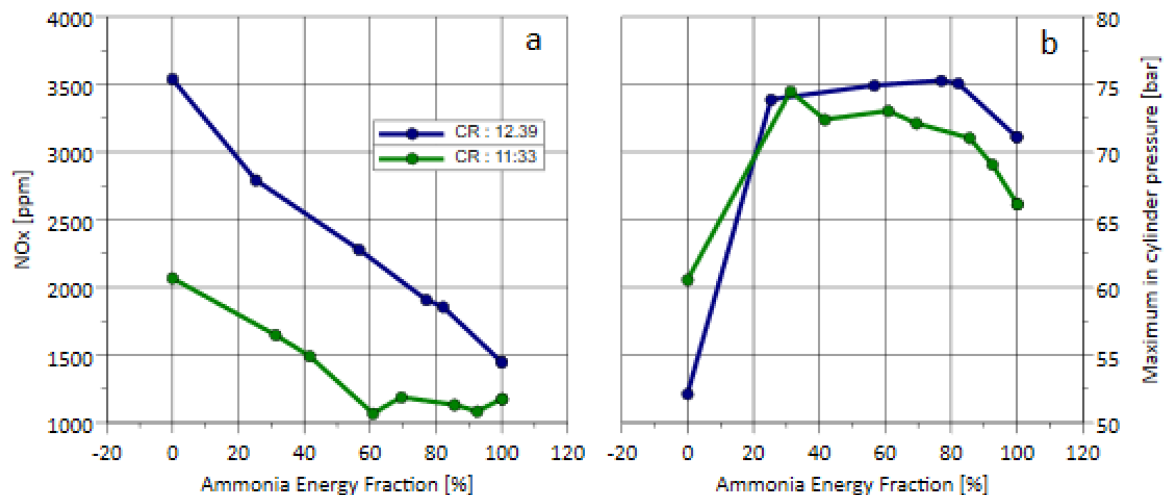
Figure 10 Variation of (a) NOx and (b) Maximum in-cylinder pressure for both configurations at different substitution ratios

The recordings of CO and total hydrocarbon (THC) emissions are set out in Figures 11(a) and 11(b) respectively. As expected, both emissions reduce with increase in ammonia substitution. While the CO emissions tended to be lower for the higher compression ratio hardware, these become identical to the old hardware beyond 60% substitution. For THC emissions, the results only diverge for 100% E10 operation and

are nearly identical for all substitutions of ammonia. Under 100% NH3 operation, the engine emissions are almost zero, the small values recorded could be from either the lubricants or due to the reading being below the accuracy limit of the emission analysers.
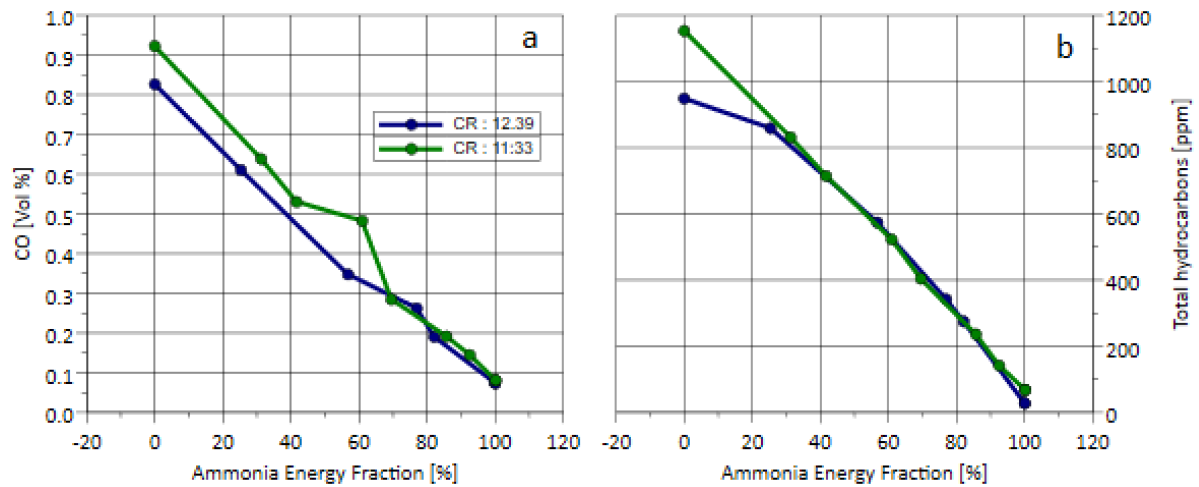

Figure 11 Variation of (a) CO and (b) THC for both configurations at different substitution ratios

Further tests were conducted with the high CR configuration at 1000, 1400 and 1800rpm with the engine load varied from 4 to 12bar IMEPn. The aim of the tests was to determine the pure ammonia speed-load map and associated impacts upon combustion, performance, fuel economy and emissions on pure ammonia operation. These tests were conducted by maintaining the same engine settings given in Table 5.

3.2   MAXIMUM SUBSTITUTION OF AMMONIA

The results of the maximum substitution of ammonia as an energy fraction of fuel at various test points are shown in Figure 12.
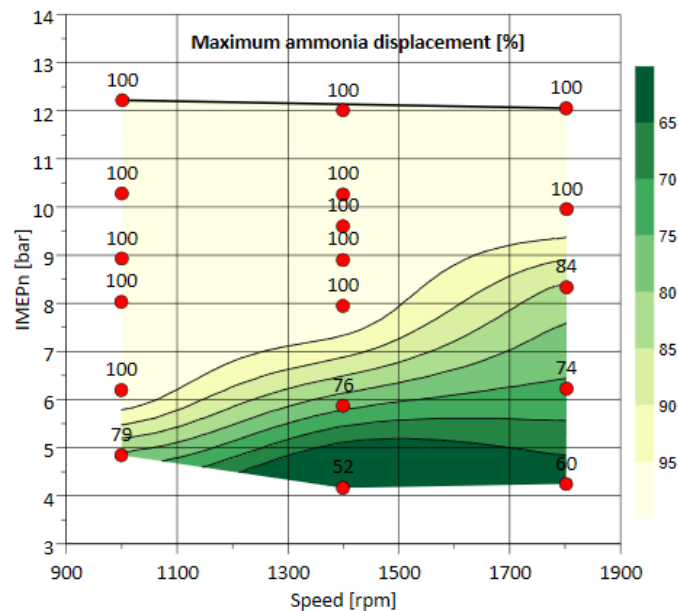
Figure 12 Maximum substitution of ammonia achieved at different load points (λ=1, MBT spark timing)

The engine was capable of operating with pure NH$_3$ even at relatively moderate engine loads. Furthermore, ammonia constituted most of the fuel energy across the map, validating the prior findings of Granell et al. [32]. The 100% substitution isoline follows a near-linear pattern, with the threshold load required to operate on pure NH$_3$ increasing by 2bar IMEPn for an increase of 400rpm in engine speed. This direct relation of threshold engine load and engine speed was also observed by Mounaïm-Rousselle et al. [26] in their work on ammonia SI engines. This trend is despite increasing gas temperatures at higher speeds and illustrates the favourable dominance in lower speed providing more time for combustion to occur despite the fact the in-

cylinder and exhaust gas temperatures usually increase with engine speed (for a given load). The impact of increasing speed and in-cylinder turbulence requires future study.

3.3 GENERAL TRENDS OF PURE AMMONIA OPERATION IN AN SI ENGINE

3.3.1 COMBUSTION

Figure 13 shows the spark timing required to achieve MBT and the corresponding stability of the engine at the tested points. Examining the map, it is evident that engine combustion stability improves considerably as the load increases from the threshold load for pure ammonia operation.
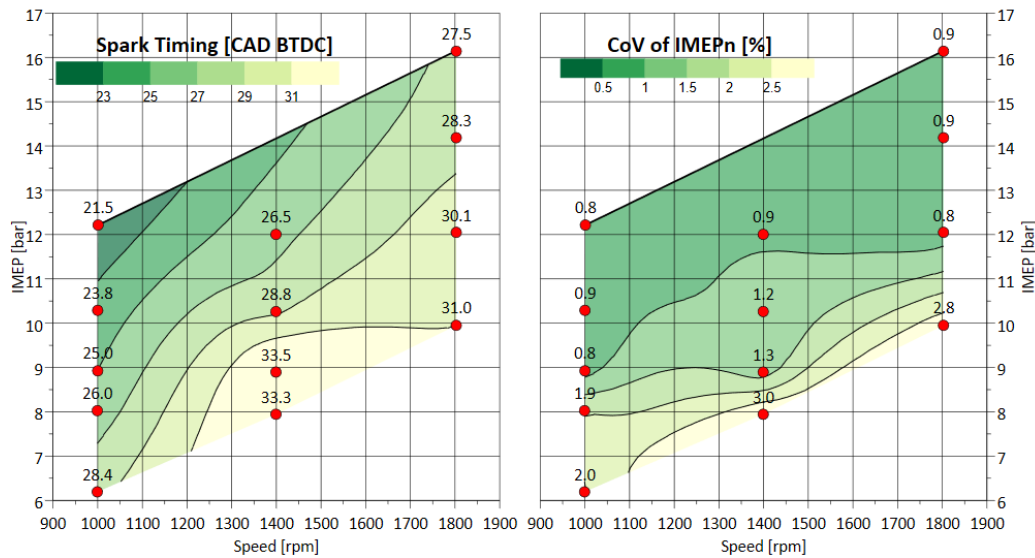

Figure 13 Spark timing and CoV of IMEPn of pure ammonia test points

The spark advance required to achieve MBT reduces with increase in load or reduction in engine speed, similarly the engine operation becomes notably more stable beyond 4bar IMEPn at all engine speeds. The mass fraction burned at the various test points is shown in Figure 14, where the "flame development phase" (0-10% MFB) followed a similar trend to the spark timing. However, the "combustion phase" (10-90% MFB) variation was relatively small for the test points. Moreover, the flame development phase was similar to the combustion phase at low speeds and became larger than the combustion phase as the speed increased. In other words, ~50% or more of the total combustion duration encompasses the flame development phase. The lack of variation in the combustion phase with speed could be a direct result of increased turbulence enabled by a high tumble head used in the study (to be confirmed in future optical engine and CFD analysis work).
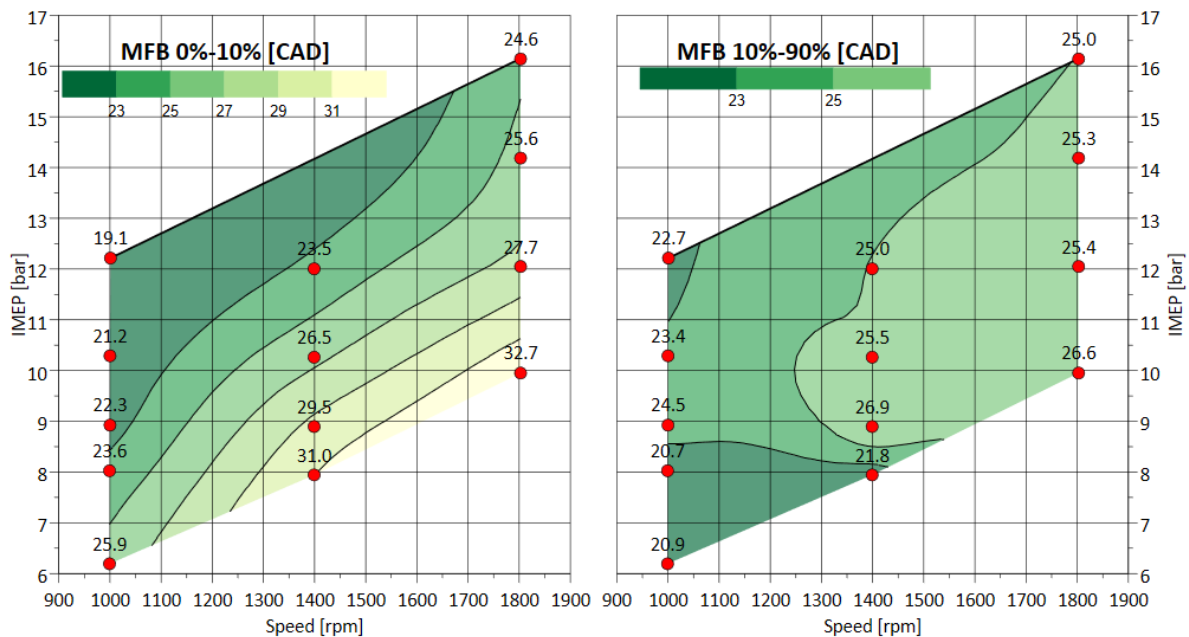

Figure 14 Variation of combustion metrics 0%-10% MFB and 10%-90% MFB for pure ammonia combustion at various speeds and loads

3.3.2 EFFICIENCY

The variation in net Indicated Thermal Efficiency (ITE) in the test region for pure NH_3 operation and pure E10 operation is set out in Figure 15. Pure NH_3 operation is considerably more efficient than E10 in the test region by virtue of ammonia having a higher octane rating and low air-fuel ratio, both of which combined enabled the engine to be operated at MBT with high loads, allowing the engine to achieve efficiencies as high as 40% at 1800rpm/16bar IMEPn, a 14% improvement over pure E10 operation under similar operating conditions.
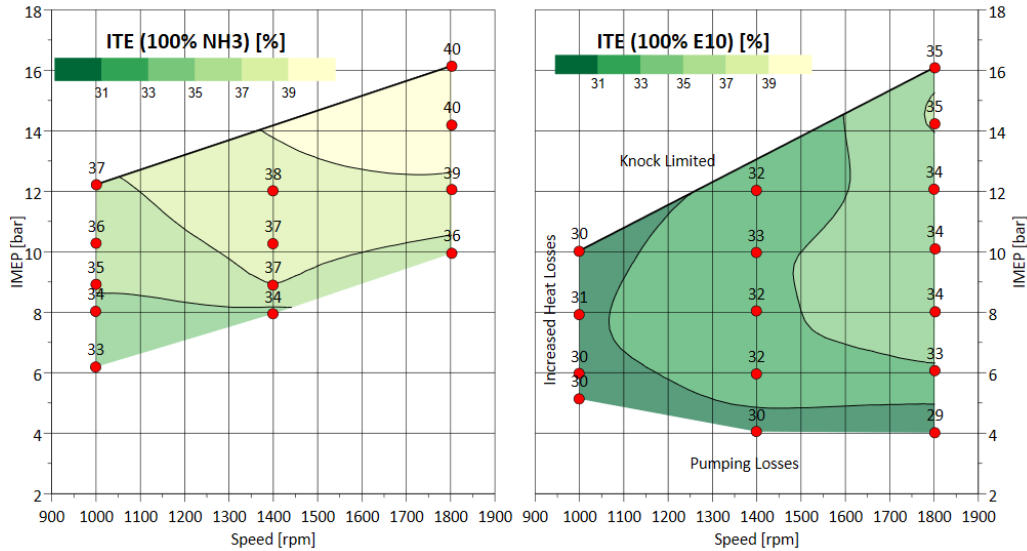

Figure 15 ITE of 100% NH₃ vs 100% E10 operation

Examining the variation of ITE for pure NH_3 operation, the efficiency improves with increase in speed and load; between them the impact of load increase is larger than that of engine speed. This variation suggests losses from increased heat rejection, pumping and knock that govern E10 operation in the test region do not directly apply to pure NH_3 operation, or these factors have minimal impact on the ITE (potentially related to the ability to achieve MBT across the map).

3.3.3 EMISSIONS

The engine-out NOx and NH_3 slip emissions from the engine operating on pure NH_3 are set out in Figure 16. NOx emissions remain relatively similar across the tested region, with the values increasing closer to the threshold load points mainly due to the advanced spark timing aiding NOx formation via increased in-cylinder temperatures. However, the emissions are nearly one third of that produced during pure E10 operation (~3000-4000ppm) under the same conditions.
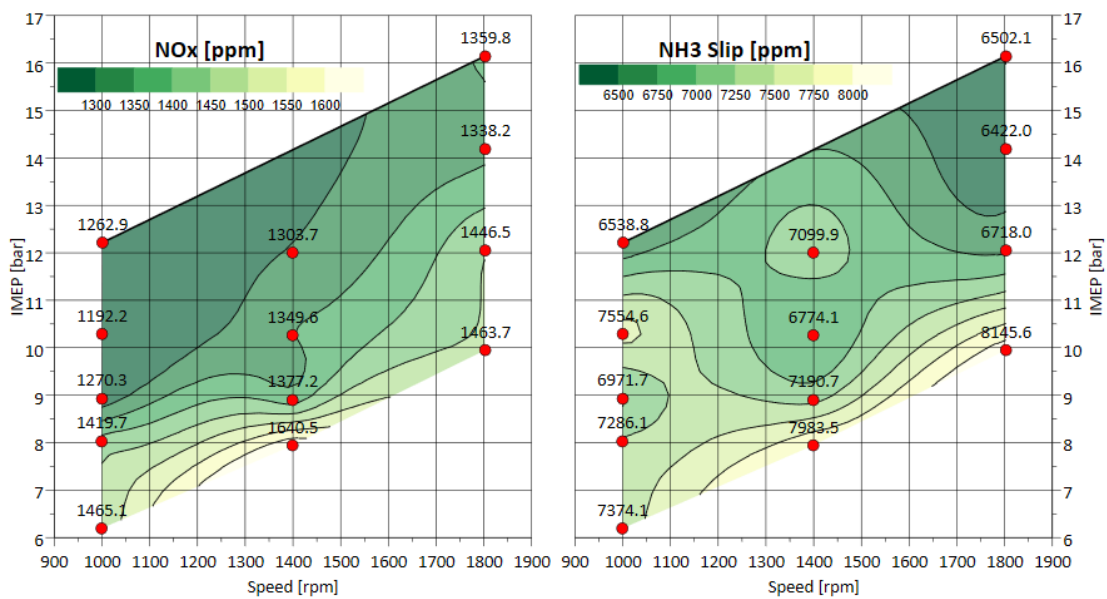

Figure 16 Emissions of NOx and ammonia slip for pure ammonia test region

Similar to NOx, ammonia slip also peaks near the threshold load from the unstable engine operation in those points. While the slip improves with engine stability, there is considerable slip (> 0.5% vol.) even in the stable operating points. The recorded NH_3 slip values are comparable to previous studies published by Lhuillier et al. and Mounaïm-Rousselle et al. [25, 37] using similar engines under similar operating conditions (λ, MBT). The two major causes for the high values of slip are (a) in-cylinder scavenging, pushing part of the injected ammonia in the intake port directly into the exhaust and (b) the incomplete combustion of ammonia trapped in crevice volumes. However, further investigations are necessary to quantify such effects. One of the potential uses of the excessive slip is to clean the NOx via a Selective Catalytic Reduction (SCR) catalyst, potentially eliminating the need for any "AdBlue" (to be confirmed in future work under leaner conditions). Moreover, high exhaust gas temperatures could enable the oxidation of excess ammonia within the catalyst as determined by Girard et al. [38]. However, the "alpha" ratio (ratio of NH_3 to NOx on a mass basis) is considerably higher than desired values between 1 and 2, which suggests the need for ammonia scrubber/oxidation catalyst to remove the excess ammonia (with potential trade-offs to be made with N_2O production).

4   CONCLUSIONS

This paper detailed experimental work undertaken to assess the feasibility of co-fuelling a modern SI engine with ammonia and E10 with two different compression ratios. The key conclusions for the work can be summarised:

- Increasing the compression ratio reduces the threshold engine load required to achieve pure ammonia operation from 12bar IMEPn to 10bar IMEPn at 1800rpm, as a result the engine operated with higher stability (0.8% vs 3% CoV of IMEPn) at 12bar IMEPn for the higher CR configuration.
- Higher CR improves the flame development phase (0-10%MFB) of the combustion with pure NH3, however co-fuelling with E10 (and potentially other fuels) negates this advantage.
- The combustion phase is slower for higher CR operation, resulting in the same spark timing for both configurations.
- The ITE is higher for the higher CR configuration, by virtue of the shorter exhaust cam extending the effective ER from 8.64 to 11.94.
- NOx emissions are higher by ~1000ppm for the higher CR configuration as a result of similar spark timings being adopted, resulting in higher in-cylinder temperatures.
- The emissions of CO and THC reduces with increased ammonia substitution and becomes identical beyond 50% ammonia substitution.

The engine was mapped with the higher CR configuration to understand the speed-load at which pure ammonia operation can be achieved and associated impact on pure ammonia operation. These tests show that:

- Under low speeds and a fully warm engine state, the engine can operate efficiently on pure ammonia at low to moderate loads.
- The threshold engine load where pure ammonia operation is achieved reduces with reduction in engine speed, reducing from 10bar IMEPn at 1800rpm to 6bar IMEPn at 1000rpm.
- Stable operation of the engine below the threshold engine load requires co-fuelling with E10, however more than 50% ammonia substitution is achieved at test points above 4bar IMEPn.
- For a given engine speed, the spark advance required to achieve MBT improves as load increases from the threshold load.
- The flame development phase (0-10% MFB) of pure ammonia combustion was identical to, or longer than, the combustion phase (10-90% MFB), with duration reducing with engine load and increasing with engine speed.
- The combustion phase using ammonia has minimal variation with load and speed changes, remaining within 4-5 CAD across the test region.
- The favourable anti-knock characteristics of ammonia enabled higher net indicated thermal efficiency (increased ITE ~5%) under pure ammonia operation compared to pure E10. No knock was encountered during testing.
- A maximum net indicated thermal efficiency of 40% was achieved at 1800rpm/16bar IMEPn, which could increase with load and speed as heat transfer losses seem to be reduced in the test region due to lower combustion temperatures.
- NOx emissions remained relatively similar (within 500ppm) across the map, with ammonia operation generally resulting in lower NOx emissions (up to 60% reduction compared to pure E10 operation). This potentially indicates significant chemical NOx formation mechanisms, rather than thermal formation mechanisms alone.
- Ammonia slip emissions were relatively high in the tested region (albeit in agreement with reports elsewhere), peaking near the threshold load points due to potentially incomplete combustion. Values for NH_3 emissions remain high (>6000ppm) even at stable operating points.

Immediate future work will focus on co-fuelling with hydrogen, accompanied by detailed breakdown of NOx species (NO, N_2O, NO_2) at varied compression ratios and relative fuel to air ratios. The engine is also being

modified to incorporate a higher stroke to bore ratio, better emulating typical heavy duty operation and also enabling higher geometric compression ratios.

5   LIST OF ABBREVATIONS

CAD: Crank Angle Degree
CR: Compression ratio
ER: Expansion ratio
CoV: Coefficient of Variance
NH$_3$: Ammonia
NOx: Oxides of Nitrogen
SI: Spark Ignition
BLD-1: Borderline detonation -1
LHV: Lower heating Value
ITE: Indicated thermal efficiency.
MFB: Mass Fraction Burned
CoV: Coefficient of Variance
IVO: Intake Valve Opening
IVC: Intake Valve Closing
EVO: Exhaust Valve Opening
EVC: Exhaust Valve Closing
E10: Gasoline with 10% ethanol
CI: Compressed Ignition
DI: Direct injection
PFI: Port fuel Injection
BTDC: Before Top dead centre
BTDCf: Before Top dead centre firing
MBT: Maximum Brake Torque
ppm: parts per million
IMEPn: Net Indicated Mean Effective Pressure
CO: Carbon Monoxide
THC: Total Hydrocarbons
RoHR: Rate of heat Release

6   DECLERATIONS

6.1   CONSENT OF PUBLICATION
Not applicable

6.2   DATA AVAILAIBILITY AND MATERIAL
The data presented in the report cannot be made available as the data is the intellectual property of Mahle Powertrains Ltd.

6.3   COMPETING INTRESETS
Not applicable

6.4   FUNDING

6.5   AUTORS CONTRIBUTIONS
AA,SG and AH conducted the experiments and collected and analysed the data in the manuscript, AA drafted the manuscript with AC, JH and MB reviewing the drafts. All authors read and approved the final manuscript

6.6   ACKNOWLEDGEMENTS

7   REFERENCE LIST

1.   IRENA. (2021). *A pathway to decarbonise the shipping sector by 2050*. Abu Dhabi. Retrieved from https://www.irena.org/Publications/2021/Oct/A-Pathway-to-Decarbonise-the-Shipping-Sector-by-2050

2.   APC UK. (2021). *Thermal Propulsion Systems Roadmap 2020*. Retrieved from https://www.apcuk.co.uk/wp-content/uploads/2021/09/https___www.apcuk_.co_.uk_app_uploads_2021_02_Exec-summary-Technology-Roadmap-Thermal-Propulsion-Systems-final.pdf

3.	Korch Emerio. (1945). Ammonia - A Fuel for Motor Buses. *Journal of Institute of Petroleum*, *31*, 213–223

4.	Gray, J. T., Dimitroff, E., Meckel, N. T., & Quillian, R. D. (1967). Ammonia Fuel — Engine Compatibility and Combustion. *SAE Transactions*, *75*, 785–807. Retrieved from http://www.jstor.org/stable/44563675

5.	Ryu, K., Zacharakis-Jutz, G. E., & Kong, S. C. (2014). Performance characteristics of compression-ignition engine using high concentration of ammonia mixed with dimethyl ether. *Applied Energy*, *113*, 488–499. https://doi.org/10.1016/J.APENERGY.2013.07.065

6.	Gross, C. W., & Kong, S. C. (2013). Performance characteristics of a compression-ignition engine using direct-injection ammonia–DME mixtures. *Fuel*, *103*, 1069–1079. https://doi.org/10.1016/J.FUEL.2012.08.026

7.	Gill, S. S., Chatha, G. S., Tsolakis, A., Golunski, S. E., & York, A. P. E. (2012). Assessing the effects of partially decarbonising a diesel engine by co-fuelling with dissociated ammonia. *International Journal of Hydrogen Energy*, *37*(7), 6074–6083. https://doi.org/10.1016/J.IJHYDENE.2011.12.137

8.	Reiter, A. J., & Kong, S. C. (2011). Combustion and emissions characteristics of compression-ignition engine using dual ammonia-diesel fuel. *Fuel*, *90*(1), 87–97. https://doi.org/10.1016/J.FUEL.2010.07.055

9.	Reiter, A. J., & Kong, S. C. (2008). Demonstration of compression-ignition engine combustion using ammonia in reducing greenhouse gas emissions. *Energy and Fuels*, *22*(5), 2963–2971. https://doi.org/10.1021/EF800140F/ASSET/IMAGES/LARGE/EF-2008-00140F_0019.JPEG

10.	Pearsall, T. J., & Garabedian, C. G. (1968). Combustion of Anhydrous Ammonia in Diesel Engines. *SAE Transactions*, *76*, 3213–3221. Retrieved from http://www.jstor.org/stable/44562853

11.	Pochet, M., Dias, V., Jeanmart, H., Verhelst, S., & Contino, F. (2017). Multifuel CHP HCCI Engine towards Flexible Power-to-fuel: Numerical Study of Operating Range. *Energy Procedia*, *105*, 1532–1538. https://doi.org/10.1016/J.EGYPRO.2017.03.468

12.	Tay, K. L., Yang, W., Li, J., Zhou, D., Yu, W., Zhao, F., … Mohan, B. (2017). Numerical investigation on the combustion and emissions of a kerosene-diesel fueled compression ignition engine assisted by ammonia fumigation. *Applied Energy*, *204*, 1476–1488. https://doi.org/10.1016/J.APENERGY.2017.03.100

13.	Starkman, E. S., Newhall, H. K., Sutton, R., Maguire, T., & Farbar, L. (1967). Ammonia as a Spark Ignition Engine Fuel: Theory and Application. *SAE Transactions*, *75*, 765–784. Retrieved from http://www.jstor.org/stable/44563674

14.	Xin, G., Ji, C., Wang, S., Meng, H., Chang, K., & Yang, J. (2022). Effect of ammonia addition on combustion and emission characteristics of hydrogen-fueled engine under lean-burn condition. *International Journal of Hydrogen Energy*, *47*(16), 9762–9774. https://doi.org/10.1016/J.IJHYDENE.2022.01.027

15.	Dinesh, M. H., & Kumar, G. N. (2022). Effects of compression and mixing ratio on NH3/H2 fueled Si engine performance, combustion stability, and emission. *Energy Conversion and Management: X*, *15*, 100269. https://doi.org/10.1016/J.ECMX.2022.100269

16.	Hong, C., Ji, C., Wang, S., Xin, G., Qiang, Y., & Yang, J. (2023). Evaluation of hydrogen injection and oxygen enrichment strategies in an ammonia-hydrogen dual-fuel engine under high compression ratio. *Fuel*, *354*, 129244. https://doi.org/10.1016/J.FUEL.2023.129244

17.	Wang, Y., Zhou, X., & Liu, L. (2021). Theoretical investigation of the combustion performance of ammonia/hydrogen mixtures on a marine diesel engine. https://doi.org/10.1016/j.ijhydene.2021.01.233

18.	Lhuillier, C., Brequigny, P., & Contino, F. (2021). Experimental investigation on ammonia combustion behavior in a spark-ignition engine by means of laminar and turbulent expanding flames. *Proceedings of the Combustion Institute*, *38*, 5859–5868. https://doi.org/10.1016/j.proci.2020.08.058

19.	Pyrc, M., Gruca, M., Tutak, W., & Jamrozik, A. (2022). Assessment of the co-combustion process of ammonia with hydrogen in a research VCR piston engine. https://doi.org/10.1016/j.ijhydene.2022.10.152

20.   Comotti, M., & Frigo, S. (2015). Hydrogen generation system for ammonia-hydrogen fuelled internal combustion engines. *International Journal of Hydrogen Energy*, *40*(33), 10673–10686. https://doi.org/10.1016/J.IJHYDENE.2015.06.080

21.   Mei, B., Zhang, J., Shi, X., Xi, Z., & Li, Y. (2021). Enhancement of ammonia combustion with partial fuel cracking strategy: Laminar flame propagation and kinetic modeling investigation of NH3/H2/N2/air mixtures up to 10 atm. *Combustion and Flame*, *231*. https://doi.org/10.1016/J.COMBUSTFLAME.2021.111472

22.   Mørch, C. S., Bjerre, A., Gøttrup, M. P., Sorenson, S. C., & Schramm, J. (2011). Ammonia/hydrogen mixtures in an SI-engine: Engine performance and analysis of a proposed fuel system. *Fuel*, *90*(2), 854–864. https://doi.org/10.1016/J.FUEL.2010.09.042

23.   Frigo, S., & Gentili, R. (2013). Analysis of the behaviour of a 4-stroke Si engine fuelled with ammonia and hydrogen. *International Journal of Hydrogen Energy*, *38*(3), 1607–1615. https://doi.org/10.1016/J.IJHYDENE.2012.10.114

24.   Frigo, S., Gentili, R., & De Angelis, F. (2014). Further insight into the possibility to fuel a SI engine with ammonia plus hydrogen. *SAE Technical Papers*, *2014*. https://doi.org/10.4271/2014-32-0082

25.   Lhuillier, C., Bréquigny, P., Contino, F., & Mounaïm-Rousselle, C. (2020). EXPERIMENTAL STUDY ON NH3/H2/AIR COMBUSTION IN SPARK-IGNITION ENGINE CONDITIONS. *Fuel*, *269*. https://doi.org/https://doi.org/10.1016/j.fuel.2020.117448

26.   Mounaïm-Rousselle, C., Mercier, A., Brequigny, P., Dumand, C., Bouriot, J., Houillé, S., & Mounaı̈m-Rousselle, C. M. (2021). Ignition engine. *Interna-tional Journal of Engine Research*, 146808742110387. https://doi.org/10.1177/14680874211038726ï

27.   Grove, J. R. (1968). THE MEASUREMENT OF QUENCHING DIAMETERS AND THEIR RELATION TO THE FLAMEPROOF GROUPING OF GASES AND VAPOURS. *Institute of Chemical engineers*, *25*.

28.   Dimitriou, P., & Javaid, R. (2020). A review of ammonia as a compression ignition engine fuel. *International Journal of Hydrogen Energy*, *45*(11), 7098–7118. https://doi.org/10.1016/J.IJHYDENE.2019.12.209

29.   Lhuillier, C., Brequigny, P., Contino, F., & Rousselle, C. (2019). Combustion Characteristics of Ammonia in a Modern Spark-Ignition Engine. *SAE Technical Papers*, (October). https://doi.org/10.4271/2019-24-0237

30.   Robinson, A. P. L., Strozzi, D. J., Davies, J. R., Kumamoto, A., Iseki, H., Ono, R., & Oda, T. (2011). Conference Series OPEN ACCESS To cite this article: Ayumi Kumamoto et al. *J. Phys.: Conf. Ser*, *301*, 12039. https://doi.org/10.1088/1742-6596/301/1/012039

31.   Ciniviz, M., & Köse, H. (2012). Academic @ Paper HYDROGEN USE IN INTERNAL COMBUSTION ENGINE: A REVIEW. *International Journal of Automotive Engineering and Technologies*, *1*, 1–15. Retrieved from www.academicpaper.org

32.   Grannell, S. M., Assanis, D. N., Bohac, S. V., & Gillespie, D. E. (2008). The fuel mix limits and efficiency of a stoichiometric, ammonia, and gasoline dual fueled spark ignition engine. *Journal of Engineering for Gas Turbines and Power*, *130*(4). https://doi.org/10.1115/1.2898837/476304

33.   Ryu, K., Zacharakis-Jutz, G. E., & Kong, S. C. (2014). Effects of gaseous ammonia direct injection on performance characteristics of a spark-ignition engine. *Applied Energy*, *116*, 206–215. https://doi.org/10.1016/J.APENERGY.2013.11.067

34.   Ryu, K., Zacharakis-Jutz, G. E., & Kong, S. C. (2014). Performance enhancement of ammonia-fueled engine by using dissociation catalyst for hydrogen generation. *International Journal of Hydrogen Energy*, *39*(5), 2390–2398. https://doi.org/10.1016/J.IJHYDENE.2013.11.098

35.   Haputhanthri, S. O., Austin, C., Maxwell, T., & Fleming, J. (2014). Ammonia and gasoline composite liquid fuel blends emulsified with ethanol and methanol for direct displacement in internal combustion engines. *IOSR Journal of Mechanical and Civil Engineering (IOSR-JMCE*, *11*(2), 11–18. Retrieved from www.iosrjournals.orgwww.iosrjournals.org

36.   Kobayashi, H., Hayakawa, A., Somarathne, K. D. K. A., & Okafor, E. C. (2019). Science and technology of ammonia combustion. *Proceedings of the Combustion Institute*, *37*(1), 109–133. https://doi.org/10.1016/J.PROCI.2018.09.029

37.   Mounaïm-Rousselle, C., Bréquigny, P., Dumand, C., & Houillé, S. (2021). Operating Limits for Ammonia Fuel Spark-Ignition Engine. *MDPI*. https://doi.org/10.3390/en14144141

38.   Girard, J., Snow, R., Cavataio, G., & Lambert, C. (2007). The influence of ammonia to NOX ratio on SCR performance. *SAE Technical Papers*. https://doi.org/10.4271/2007-01-1581